Icarus 390 (2023) 115299

Contents lists available at ScienceDirect

Icarus

journal homepage: www.elsevier.com/locate/icarus

Research Paper

Thermally induced phase transition of troilite during Micro-Raman spectroscopy analysis

Xiaoguang Li [a], Yi Chen [a,*], Xu Tang [b], Lixin Gu [b], Jiangyan Yuan [a], Wen Su [a], Hengci Tian [c], Huiqian Luo [d], Shuhui Cai [a], Sridhar Komarneni [e]

[a] State Key Laboratory of Lithospheric Evolution, Institute of Geology and Geophysics, Chinese Academy of Sciences, Beijing 100029, China
[b] Electron Microscope Laboratory, Institute of Geology and Geophysics, Chinese Academy of Sciences, Beijing 100029, China
[c] Key Laboratory of Earth and Planetary Physics, Institute of Geology and Geophysics, Chinese Academy of Sciences, Beijing 100029, China
[d] Beijing National Laboratory for Condensed Matter Physics, Institute of Physics, Chinese Academy of Sciences, Beijing 100190, China
[e] Department of Ecosystem Science and Management and Materials Research Institute, 204 Energy and the Environment Laboratory, The Pennsylvania State University, University Park, PA 16802, USA

ARTICLE INFO

Keywords:
Troilite
Raman spectroscopy
Laser irradiation
Magnetite
Nanophase metallic iron

ABSTRACT

Troilite is one type of FeS polymorph formed under reducing environmental conditions. However, its phase transition by laser heating during Raman analysis has not been investigated in detail. This study focuses on identifying changes to Raman spectra of troilite resulted by laser heating during Raman analysis so as to determine optimized analytical conditions for characterizing iron sulfides. We comfirm that iron sulfides exposed in air are easily transformed to magnetite and hematite after a high-power laser ($>$ 200 mW/μm^2 for pyrite and $>$ 14 mW/μm^2 for troilite) irradiation. Troilite crystal structure is also broken easily by laser ($>$12 mW/μm^2) under the vacuum conditions due to the volatilization of S and Fe, possibly inducing the formation of nanophase metallic iron. Therefore, iron sulfides are expected to be sensitive to laser heating. Here, we have confirmed the laser heating effect through a set of heating experiments from ambient temperature to 500 °C with various laser powers. Our results suggest that Raman analysis for troilite should be performed with a low laser power of $<$1.50 mW (12 mW/μm^2) both in air and vacuum environments. The heating effects on troilite phase transition can be responsible for the formation of magnetite, hematite, and nanophase metallic iron in lunar samples. The thermally induced phase transition of troilite observed in this study is important because it undoubtedly modifies both the redox state and magnetic property of extraterrestrial samples and would trigger a misleading interpretation of planetary evolution.

1. Introduction

Troilite, a pseudomorph of FeS commonly found on the Moon, Martian surfaces, extraterrestrial meteorites and Earth (Carpenter and Desborough, 1964; Evans, 1970; Jacob et al., 2004; Moreau et al., 2022; Münker et al., 2017; Skinner et al., 2004; Thomas et al., 2003), plays a crucial role in early solar system chronology (Tachibana and Huss, 2003), shock-induced metamorphism (Bennett III and McSween, 1996; Harries and Langenhorst, 2013; Scott, 1982), geothermometers (Skinner and Luce, 1971), the origin of life (Matamoros-Veloza et al., 2018; Onufrienok et al., 2020), and designing new-type of catalysts (Schaible et al., 2019; Zhou et al., 2019).

Raman spectroscopy was usually employed to identify mineral polymorphs for both terrestrial and extraterrestrial samples (Minitti et al., 2005; Neuville et al., 2014; Wang et al., 2015). However, most metallic minerals are insensitive to Raman spectroscopy because of their poor light scattering characteristics (de Faria et al., 1997; Sharma et al., 2009). Therefore, high laser power is usually used to identify iron sulfide minerals (Mernagh and Trudu, 1993; Wang et al., 1999). Laser power could induce an increase the local temperature on the sample surface (Sahoo et al., 2013), making sulfides oxidized easily at high temperatures (Genchev and Erbe, 2016; Onufrienok et al., 2020; Weber et al., 2017). To date, only a few Raman spectroscopy studies on troilite have been conducted due to the vulnerability of Fe—S bond (Avril et al., 2013; Matamoros-Veloza et al., 2018; Weber et al., 2017). For example, Weber et al. (2017) found that Raman measurements on troilite in

* Corresponding author.
E-mail address: chenyi@mail.iggcas.ac.cn (Y. Chen).

https://doi.org/10.1016/j.icarus.2022.115299
Received 12 May 2022; Received in revised form 6 September 2022; Accepted 3 October 2022
Available online 10 October 2022

vacuum are only feasible with a laser power of ~7 mW, corresponding to an energy density of 5.3 mW/μm^2. However, the alteration of chemical compositions and phase transitions caused by laser heating during Raman analysis has not been particularly investigated.

The content of Fe^{3+} in troilite is zero or, at least, extremely low (El Goresy, 2018; Brounce et al., 2019), pointing to a strongly reducing environment (Cameron, 1970). However, previous studies indicate that troilite is easily transformed to other phases with changing redox state. Either weathering or sample preparation of troilite may lead to the oxidation of Fe^{2+} to Fe^{3+} (Shearer et al., 2014; Taylor and Burton, 1976; Taylor et al., 1974). For example, some Fe-bearing minerals in extra-terrestrial samples may be altered by the ambient environment on Earth (Chen et al., 2002; Prieto-delaVega et al., 2022; Wesełucha-Birczyńska and Żmudzka, 2008). In vacuum environment, both meteorite impaction and solar wind can alter the redox states of iron and sulfur in troilite (Tachibana and Huss, 2005; Gu et al., 2022). Troilite is commonly associated with metallic Fe^0 (or Fe—Ni metal) in impact breccias and exhibits a shearing boundary between them (Begemann and Wlotzka, 1969; Boctor et al., 1982; Chen et al., 2002), suggesting a genetic chain between troilite and metallic Fe^0 during shock metamorphism. In addition, several studies suggest that stoichiometric FeS as a metastable intermediate phase would decompose upon space weathering or heating (Brounce et al., 2019; Fei et al., 1997). Therefore, change in heating or weathering environments would induce troilite phase transition and thus adjust the valence state of iron. The Moon's paleomagnetic field, an essential restrictive condition of the lunar evolution, can be detected in lunar samples via thermoremanent magnetization experiments at temperatures above 700 °C (Tarduno et al., 2021). However, how temperature affects the magnetic property of troilite during these heating experiments is still unknown. The sample preparation and experimental procedure should be kept out of oxygen to avoid surface oxidation, which may lead to misleading magnetic results.

Here, we focus on the mechanism of laser irradiation-induced phase transformations of troilite. We found that troilite is sensitive to laser heat in both vacuum and ambient air conditions. Heating experiments further test the stability of iron sulfide under various temperatures. Our results would provide new insights into the origins of lunar iron oxides and nano metallic iron, both of which would affect the magnetic properties of lunar samples.

2. Experimental

2.1. Samples

Troilite is found in a Dar el Kahal H5–6 ordinary meteorite sample, which mainly consists pyroxene, olivine, plagioclase, apatite, troilite and Fe—Ni metal. The meteorite sample was embedded in an epoxy mount and polished with diamond paste. The visual characteristics of the meteorite sample grains are shown in Fig. 1. The SEM pictures reveal that the anhedral troilite occurs in veins and droplets inside the pyroxene and olivine. The troilite granules are usually directly connected to the Fe—Ni metal, which indicates possible formation through shock-induced metamorphism with a shock stage of S4-S5 (Miyahara et al., 2020; Stöffler et al., 1991). In order to simulate the oxidation reaction of Fe, destructive in situ heating experiments were carried out using pyrite, hematite, and magnetite, which were collected from Guangdong province, Guangxi province, and Inner Mongolia autonomous region, China, respectively. The pyrite shows light copper yellow color, opaque, and 1.0 cm euhedral cube crystal morphology. The hematite was formed in a sedimentary environment with a kidney shaped morphology and dark red color. The magnetite shows an iron black color and magnetic characteristics. The Fe-bearing samples were polished along one random plane with 9 μm, 3 μm, and 1 μm diamond slurry, respectively prior to observation.

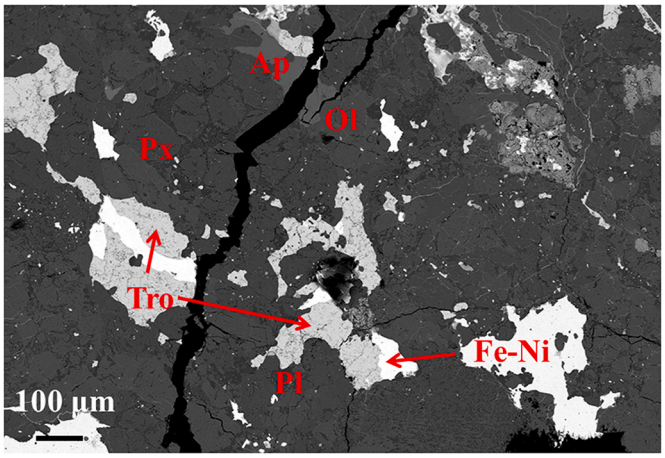

Fig. 1. Back-scattered electron (BSE) image of the meteorite. Tro = troilite, Pl = plagioclase, Px = pyroxene, Ol = olivine, Ap = apatite, Fe-Ni = Fe-Ni metal.

2.2. Instrumentation and operating conditions

2.2.1. Micro-Raman spectroscopy

Micro-Raman spectroscopy was performed by a Witec alpha300R confocal Raman microscope and a Raman Imaging and Scanning Electron Microscopy system (RISE system consists of a Zeiss Gemini 450 SEM and a Witec alpha300R Raman) at the Institute of Geology and Geophysics, Chinese Academy of Sciences(IGGCAS).

The Raman measurements were carried out under both ambient and 2.99×10^{-6} mbar vacuum conditions (RISE system). The sample can be transferred between the SEM and Raman measuring positions within the vacuum chamber of the Gemini 450 SEM. SEM image was acquired using the BSE detector of the RISE system and light microscopy modes were applied when conducting the Raman test. Samples for Raman measurement were not coated with carbon.

The spectra were excited with 532 nm radiation from a semiconductor laser with a ~ 0.02 nm spectra width (FWHM). A 600 grooves/mm grating with a spectral resolution of 3 cm^{-1} was used. The laser beam was focused on the sample surface by a 100× Zeiss microscope (NA = 0.9 in air and 0.7 in a vacuum, with a spot size of ca. 360 nm and 460 nm). We have made an estimation of 8 mW/μm^2 irradation energy on the sample by 1 mW laser (Fig. 2). The Raman shift regions of 80– 1600 cm^{-1} were used for this study, and the data has been calibrated with a silicon peak of 520.7 cm^{-1}. A spectral acquisition time of 5– 40 s and total spectra with 20– 50 accumulations were collected for each measurement. The spectra were not baseline corrected.

2.2.2. Scanning Electron Microscope (SEM) and energy-dispersive X-ray spectroscopy (EDS)

SEM and EDS analyses were performed at IGGCAS. A high-resolution field emission scanning electron microscope (Zeiss Gemini 450) operating at 15 kV and beam current of 2 nA was used to perform visualization and imaging of the microstructure of samples. To eliminate charging and improve the contrast for low-density materials, a carbon coating of about 8 nm was performed at the coater system (Leica EM ACE600) to facilitate high-resolution FESEM imaging. To reveal the elemental distribution of samples, EDS data were collected with Oxford Ultim Max 60 mm^2 EDS detectors attached to SEM at 15 kV.

2.2.3. Focused ion beam–scanning electron microscope (FIB–SEM) and Transmission Electron Microscope (TEM)

The electron-transparent foil with typical dimensions of 4.5 × 6.0 × 0.1 μm (Fig. 3–a) was prepared using a Zeiss Auriga Compact FIB-SEM at IGGCAS. Ion beam conditions for the final thinning and polishing were 5–30 kV high voltage with beam currents of 50 pA–2 nA. The TEM foil

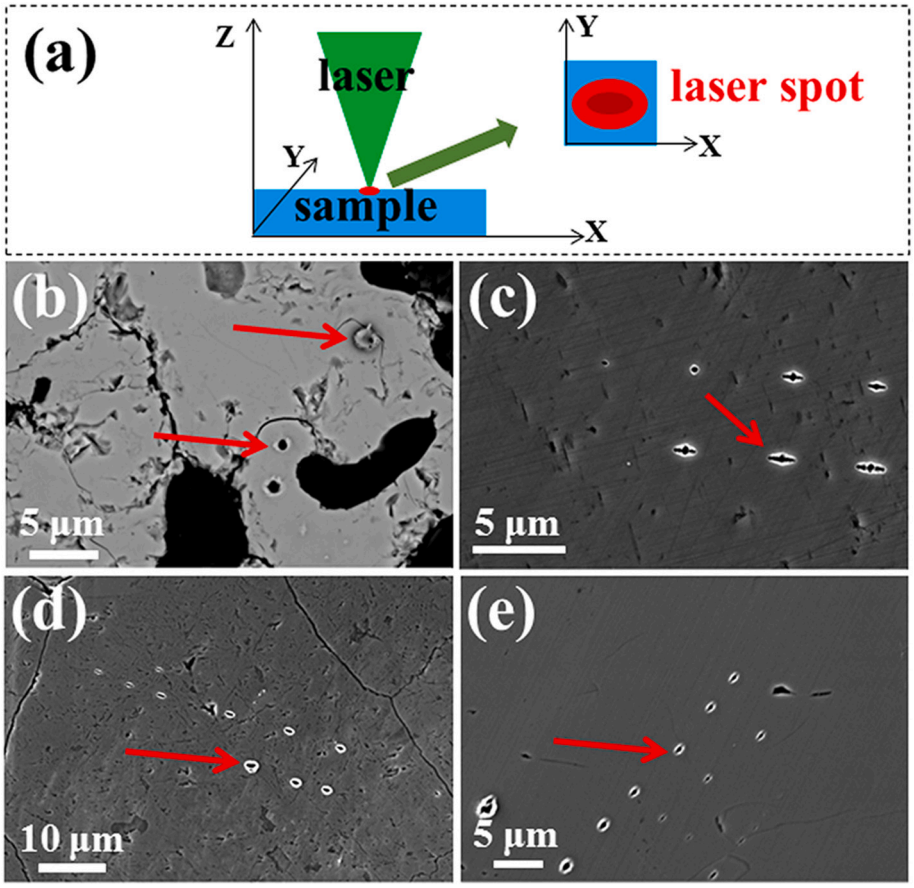

Fig. 2. (a) Schematic drawing of the laser path; Back-scattered electron (BSE) images of (b) troilite, (c) pyrite, (d) hematite, (e) magnetite (Red arrows show the laser points). (For interpretation of the references to color in this figure legend, the reader is referred to the web version of this article.)

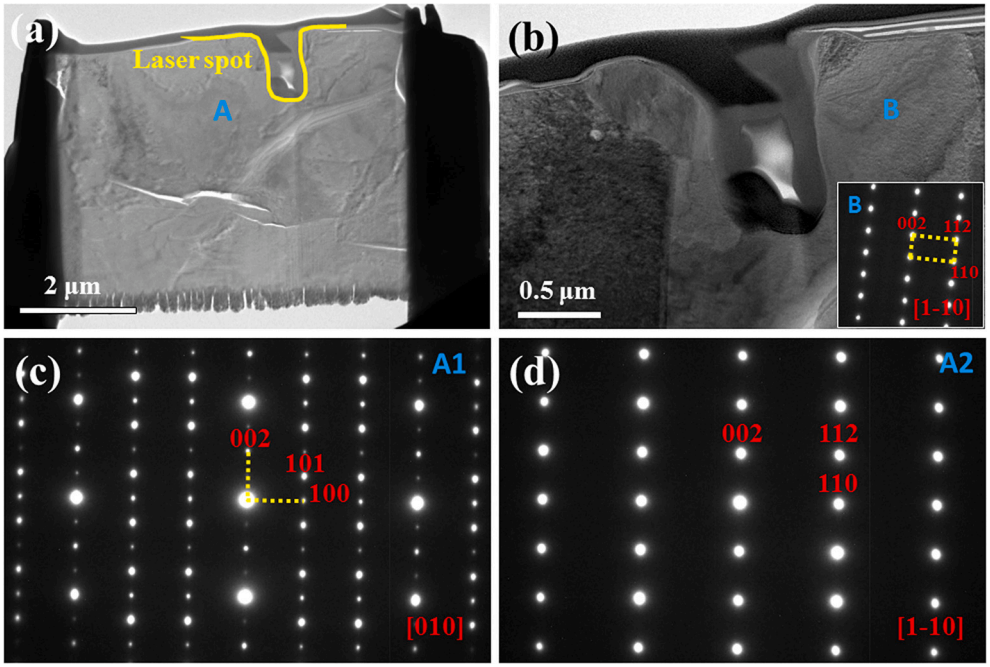

Fig. 3. Analysis of FIB foil taken from the laser point generated in vacuum. (a) BF-TEM image of the slice made by FIB-SEM; (b) HRTEM of the laser spot and a SAED pattern of the B area view along [1–10]; (c) and (d) SAED pattern of A area viewed along the [010] and [1–10] direction.

was then attached to a copper grid by the Omniprobe AutoProbe200 micromanipulator. The copper grid with prepared foil was fixed on a TEM holder for TEM observation and analysis. The TEM bright-field imaging, selected area electron diffraction (SAED) and high-resolution transmission electron microscopy (HRTEM) imaging were performed using a JEOL JEM-2100 TEM at IGGCAS, with the electron beam generated from a LaB6 gun and operating voltage of 200 kV. The BF-TEM images show that the laser spot (Fig. 3–b) has a diameter of 0.56 μm and a depth of 1.3 μm. Fig. 3–c and d show the SAED pattern of the selected area A viewed along the [010] and [1−10] directions, respectively.

2.2.4. Heating experiments

The effect of temperature on the Raman spectrum of the samples was investigated using a Linkam TS 1400XY heating stage (Linkam Scientific Instruments) at IGGCAS. The samples with a thickness of ~0.5 mm were put in a tubular platinum furnace covered by ceramic. In situ heating experiments were conducted from 25 °C to 500 °C in air with a 100 °C interval. The heating procedure was regulated manually by Linksys32 softeware controller with a 60 °C/min heating rates. The temperature accuracy and stability are ±1 °C. Air is circulated at a flow rate of ~6 ml/min through the furnace during the test. The sample wafer was placed on a sapphire disc within the temperature stage. The upper window of the temperature stage is made of zinc selenide and the lower window is of quartz. Every test was conducted after 5 min of temperature retention.

3. Results

3.1. Thermally induced oxidation of troilite in air

We have identified the typical troilite crystal structure by TEM-SAED (Fig. 3–b,–c,–d). Troilite has a NiAs-type crystal structure with a hexagonal unit cell. In the crystal structure of troilite, Fe atom located in the octahedral pores, is surrounded by six S atoms with a distance of 0.2359 nm to 0.2721 nm (Evans, 1970), producing different vibration modes. Fig. 4 shows the Raman spectra of troilite in air at different laser powers. Raman spectroscopic analysis revealed that the typical troilite Raman shifts at around 148 cm^{-1}, 197 cm^{-1}, 228 cm^{-1}, 255 cm^{-1}, and 308–331 cm^{-1}, which are due to the S—S and Fe—S vibrations. It was reported that pyrrhotite ($Fe_{1-x}S$) exhibits peaks according to the stoichiometric composition and most of the Fe—S bands are in the region of

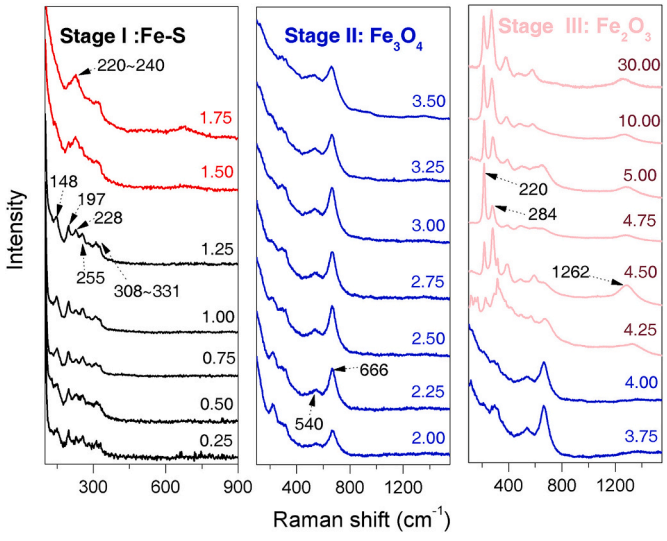

Fig. 4. The Raman spectra of troilite with different laser powers in air (the numbers show the laser energy with an interval of 0.25 between 0.25 mW and 5.00 mW).

200– 400 cm^{-1} (Wopenka, 2012). The dominant Raman bands of S are reported as 153 cm^{-1} and 187 cm^{-1} (White, 2009). As shown in Fig. 4, the high laser +power led to a clear change of the spectrum of the troilite. The 148 cm^{-1} and 197 cm^{-1} peaks, which can be assigned to S—S vibrations, show a blue shift with increasing temperature but disappeared when laser power went up to 1.75 mW (Fig. 4). The new Raman peaks formed in 220– 240 cm^{-1} (stage I) occurred at 1.50 mW, which should not be assigned to the Fe or S vibrations of oxidation phase because similar peaks also formed under vacuum conditions. A 240 cm^{-1} Raman peak was once observed on synthetic troilite and meteorite troilite at −263 °C (Avril et al., 2013). The band in the 220– 240 cm^{-1} region observed previously (Weber et al., 2017) is due to Fe—S band bending accordingly (Stage I in Fig. 4). The Raman spectrum of troilite corresponds to the peaks of magnetite (Stage II in Fig. 4), showing that a transition of FeS into Fe_3O_4 with the main peak occurring around 666 cm^{-1} and additional low-intensity peaks around 540 cm^{-1} at 2.00 mW during laser enhancement process. The Fe was oxidized under the high temperature induced by the laser. The magnetite phase was transformed into hematite (Stage III in Fig. 4) at 4.25 mW or higher power.

As determined by EDS (Fig. 5), the predominant elements in the troilite samples were Fe and S. The S—S and Fe—S bonds of the troilite were likely to be broken when they were irradiated. The elemental data of the laser spot indicated that the troilite was oxidized after laser irradiation, and the S was volatilized in the form of SO_2. As a consequence, the Fe^{2+} was in-situ fixed in the form of magnetite and hematite if O element existed (Fig. 6). The possible reaction sequence is listed as follows:

$$FeS + O_2 \rightarrow Fe_3O_4 + SO_2 \ (\text{Stage II}) \quad (1)$$

$$FeO + O_2 \rightarrow Fe_2O_3 + SO_2 \ (\text{Stage III}) \quad (2)$$

3.2. Thermally induced oxidation of Fe-bearing minerals in air

In order to figure out the thermal-induced oxidation behavior of Fe^{2+} during the Raman measurement, different laser powers were used to simulate the phase transition reaction. Moreover, a rough correlation between laser power and the associated temperature during the measurement was established based on in situ heating experiments of the selected Fe-bearing minerals.

Pyrite, hematite, and magnetite are mainly composed of Fe, S, and O elements with the stoichiometric formula of FeS_2, Fe_2O_3, and Fe_3O_4, respectively. The main Raman peaks are localized at 351 cm^{-1}, 384 cm^{-1}, and 441 cm^{-1} for the pyrite (Fig. 7–a), at 227, 295, 411, and 1317 cm^{-1} for the hematite (Fig. 7–b) and at 311, 570, and 672 cm^{-1} for the magnetite (Fig. 7–c). The spectral data obtained in this study correspond well with the data reported previously in the literature (de Faria and Lopes, 2007; Marshall and Marshall, 2011; Udayabhaskar et al., 2012).

The Raman peaks of pyrite and magnetite shift to lower wavenumbers as laser power increase, indicating that the vibration energy was weakened by the thermal expansion effect (Fig. 7). However, the hematite resisted the thermal influence by its stronger molecular structure (Fig. 7–b). Locations of Raman peaks of hematite stayed constant during the experiment. Raman spectra of an in situ heated sample indicate that the 209–219 cm^{-1} and 270–289 cm^{-1} peaks (Fig. 7–b) come from the vibration of hematite from a high-temperature environment (Fig. 8–b). The Raman peaks of pyrite may shift 5– 9 cm^{-1} depending on the testing temperature and atmospheric conditions (Bryant et al., 2018; Weber et al., 2017). It was previously reported that heat-induced transformations from Raman spectroscopy significantly changed the spectrum of iron sulfide (Genchev and Erbe, 2016). In our experiments, Raman peaks of the pyrite shifted to 348 cm^{-1}, 379 cm^{-1}, and 435 cm^{-1} when a 20.0 mW laser was applied. Phase transition occurred at 25.00 mW with two new peaks at 220 cm^{-1} and 284 cm^{-1}, which indicate that the iron was oxidized (Fig. 7–a). Repeated Raman testing in this research has also proved that the newly formed phase is

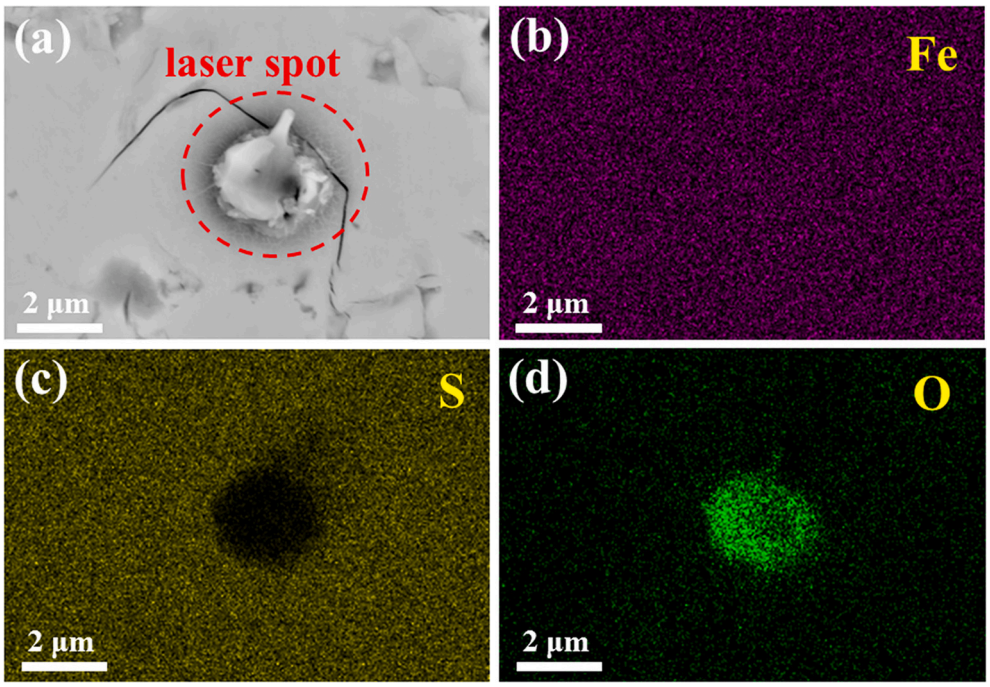

Fig. 5. (a) SEM image of the irradiated spot of troilite by 35 mW laser in air; (b), (c), (d): Fe, S, O elemental EDS mapping images of the irradiated spot, respectively.

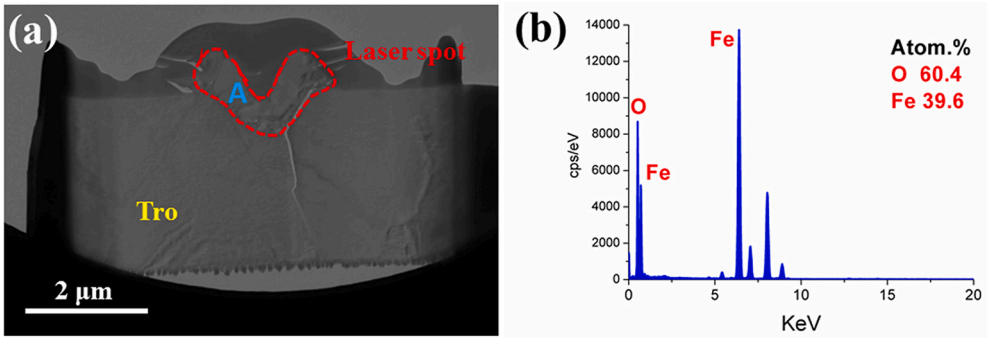

Fig. 6. Analysis of FIB foil taken from the laser point generated in air. (a) BF-TEM image of the slice made by FIB-SEM; (b) EDS of the laser spot area marked "A".

the same as hematite (Fig. 8–a). The two new Raman peaks at 216 cm^{-1} and 278 cm^{-1} of magnetite (Fig. 7–c) suggest the formation of hematite, which is consistent with the hematite reference data in the RRUFF database (Wang et al., 2004). This reaction sequence of the thermal transformations is considered analogous with the mechanism proposed by Mitchell (2002) and Weber et al. (2017):

$$FeS_2 + O_2 \rightarrow Fe_2O_3 + SO_2 \quad (3)$$

$$Fe_3O_4 + O_2 \rightarrow Fe_2O_3 \quad (4)$$

The temperature of the laser spot can be several hundreds of degrees, even when several tens of mW power was used (Shebanova and Lazor, 2003). Raman peaks of pyrite were unchanged until 25.0 mW, while the oxidation peaks of magnetite started at ~5.0 mW (Fig. 7). Compared with pyrite and hematite, magnetite is more likely to suffer from irradiation alterations. Similar Raman frequency shifts were also observed in the studies on nanosized hematite (Owens and Orosz, 2006), magnetite (Moldenhauer et al., 2018), and Martian meteorite (Wang et al., 2004).

In situ heating experiments were further used to verify the irradiation effect. The sample was heated from 26 °C to 500 °C at regular temperature intervals. The observed spectrum at 400 °C is similar to that of the laser-irradiated samples, indicating that the transformation came from the thermal effect of the laser. The transition temperature of pyrite and magnetite is about 400 °C (Fig. 8). As expected, the spectral changes are irreversible, as shown in Fig. 9. Therefore, we concluded that the temperature controls the occurrence and progress of the oxidation reaction. The correct use of laser power is a prerequisite for reliable Raman spectra of Fe-bearing mineral systems.

3.3. Thermally induced phase transformation of troilite in vacuum

For the purpose of eliminating the interference of oxygen element, the Raman test of troilite in a vacuum environment was carried out (Fig. 10). Thermal phase transition induced by irradiation cannot occur in a vacuum due to lack of oxygen. The Raman spectrum comprises of an intense band at 200–260 cm^{-1} (Stage I in Fig. 10) and it is assigned to the characteristic features of Fe—S stretching, which decreased slightly with the increasing of laser power. Raman spectrum in the Fe—S region comprises an intense band at ~220 cm^{-1}. This indicates the crystallization breakage of troilite induced by laser irradiation at ca. 4.25 mW, resulting in the loss of some mineral component, most probably the loss of S due to its volatility. This phenomenon can be observed by elemental analysis with EDS (Figs. 3 and 11). The 220 cm^{-1} band disappeared at the laser spot when 5.0 mW laser power was applied (Fig. 10). A hollow hole at the laser spot that appeared in the vacuum measurement sample

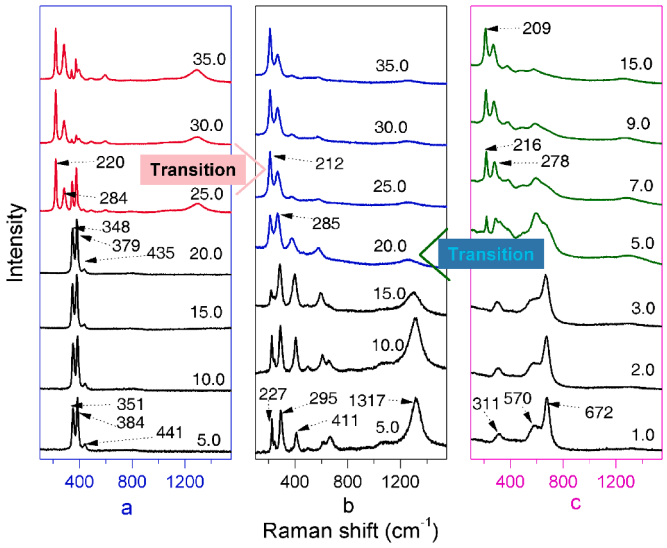

Fig. 7. The Raman spectra of three types of Fe-bearing minerals with different laser powers (a) pyrite; (b) hematite; (c) magnetite. (the numbers show the laser energy in a unit of mW).

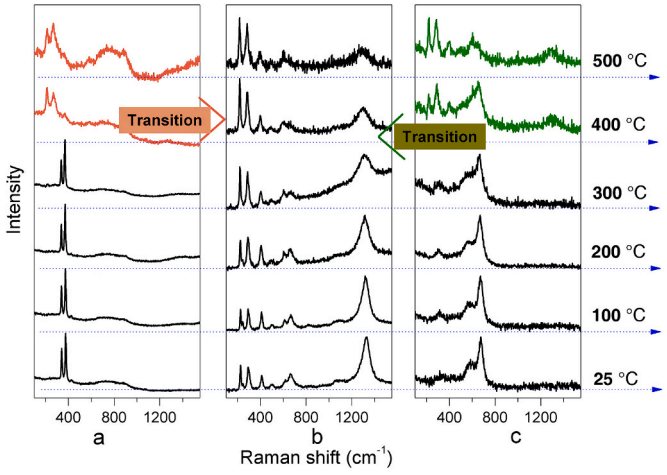

Fig. 8. In situ Raman spectra of three types of Fe-bearing minerals with different temperatures (Laser power: 2.0 mW) (a) pyrite; (b) hematite; (c) magnetite.

can be observed from the SEM (Fig. 11) and TEM image of the FIB-cut slice (Fig. 3–a, –b). EDS signal of Fe should also be absent because the laser spot is empty. The reason for this may be assigned to the signal responding difference between Fe and S. Further study should be carried out on the elemental-related signal counting difference in the EDS measurement.

4. Discussion

4.1. The temperature effect on troilite structure

Our study presents new insights into the stability of troilite in various thermal environments. The critical point of phase transition of troilite starts at 1.50– 1.75 mW (12– 14 mW/μm^2), while it is 25.00 mW for pyrite and 5.00 mW for magnetite. This discrepancy reflects that troilite is more sensitive to laser heat than pyrite and magnetite. Different from troilite, the Fe^{2+} of pyrite is coordinated to six S in a distorted octahedral arrangement. Each S is coordinated to one S and three Fe^{2+} in a distorted tetrahedral arrangement, forming a 0.226 nm length of Fe—S bond

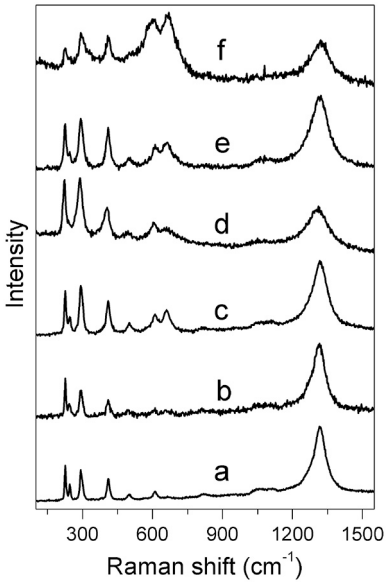

Fig. 9. The Raman spectra of (a) pyrite, (b) hematite, (c) magnetite after 35.00 mW laser irradiation; (d) pyrite, (e) hematite, (f) magnetite after 500 °C heating. (All the data in Fig. 9 were acquired with a 2 mW laser power at ambient temperature).

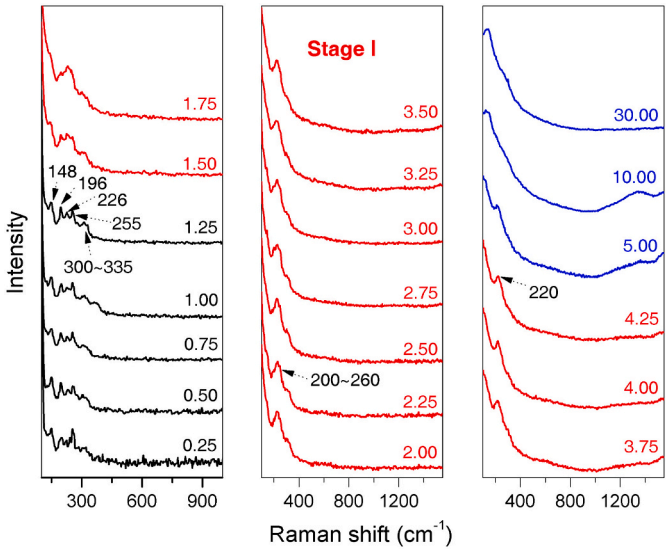

Fig. 10. The Raman spectra of troilite exposed to different laser powers in vacuum. (the numbers show the laser energy with an interval of 0.25 between 0.25 mW and 4.25 mW).

(Fleet, 1970; Nickel, 1968; Qian et al., 2010). Considering the bonding strength factor, much more energy is needed to broke the Fe—S bond of pyrite than troilite although they are both composed of Fe and S. Besides, the Crystal Orbital Hamilton Population of the Fe—S bonds and the Fe bond valence of troilite were smaller than that of pyrite, resulting in weaker bonding stability (Liu et al., 2019; Terranova et al., 2018).

The transition should not only depend on laser power but also on the instrument's setting and sample character (Foucher, 2022; Prince et al., 2020). Compared to bulk minerals with a flat plane, smaller samples with a coarse surface and dark color are easier to absorb laser energy (Bryant et al., 2018; Hanesch, 2009). The thermal effect will become severe because of the poor heat conduction of the small particles. The iron black color accounts for the high laser energy absorption efficiency of the magnetite than pyrite.

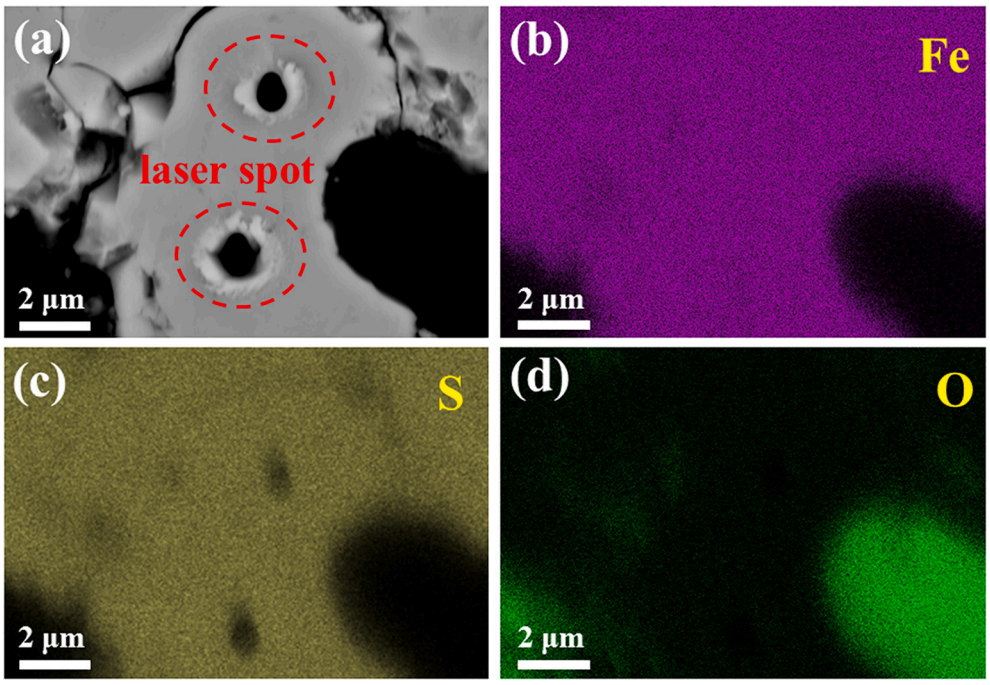

Fig. 11. (a) SEM image of the irradiated spot of troilite by 35 mW laser in vacuum; (b), (c), (d): Fe, S, O elemental EDS mapping images of the irradiated spot, respectively.

Although we cannot obtain the temperature of troilite transition directly, the heating experiments could provide equivalent information. Our experiments show that the thermally induced oxidation of pyrite and magnetite occurred around 400 °C (Fig. 8). The Raman analyses show that the corresponding transition from magnetite to hematite happened approximately at 4 mW (Figs. 4 and 7). In this regard, the phase transition of troilite caused by the 1.50 mW laser energy (Figs. 4 and 10) would most likely correspond to temperatures far below 400 °C, as laser heating is positively related to its energy.

Therefore, special technical procedures should be applied when in situ Raman measurement of troilite was carried out on planetary surface exploration (Wang et al., 2004). We suggest that the Raman analysis of troilite should be conducted with the laser power lower than 1.5 mW. Otherwise, phase transition during Raman analyses would occur and thus generate misleading results.

4.2. On the origin of lunar magnetite and hematite

The lunar surface and interior are generally thought to be highly reduced with oxygen fugacity ranging from +0.2 to −2.5 log units relative to the Fe-wüstite (IW) buffer (Wadhwa, 2008). However, this point was challenged by the detection of magnetite and hematite in lunar rocks and soils (Bell et al., 1974; Dąbrowski et al., 2008; Forester, 1973; Griscom and Marquardt, 1972; Joy et al., 2015; Kolopus et al., 1971; Pasieczna-Patkowska et al., 2008; Runcorn et al., 1971; Shearer et al., 2014; Weeks, 1972; Weeks et al., 1972; Weeks et al., 1970). These findings were used to propose that localized, variable oxidation states might occur in lunar history. However, the observation of hematite by Raman measurements is likely caused by the oxidation of lunar ilmenite or nanophase iron Fe^0 when heated in air with a laser power higher than 3 mW (Ling et al., 2011; Shearer et al., 2014). Our study further indicates that troilite is more sensitive to laser heat than ilmenite, a >1.5 mW laser power is sufficient to induce the transition from troilite to magnetite and then hematite. Therefore, the Raman detection of magnetite and hematite in lunar samples, especially close to the troilite domains, should be re-evaluated and interpreted with caution.

The presence of magnetite was well identified in Apollo 16 regolith breccia 60016 using multiple analytical techniques (Joy et al., 2015). The magnetite and troilite show a clear intergrowth texture and occur as interstitial phases surrounding the fragments of plagioclase, which was interpreted to result from impact thermal oxidation of troilite in the presence of H_2O or CO_2 (Joy et al., 2015). Our experiment shows that troilite could be also oxidized to magnetite with an addition of oxygen at low temperatures (<400 °C). This could be a complementary mechanism to generate magnetite in lunar regolith. It is worth noting that the lunar regolith can hold water, CO_2, oxygen and other volatile resources acquired from solar winds (Fagents et al., 2010; von Steiger et al., 2010) or Earth's atmosphere (Terada et al., 2017) over some 4 billion years (Barboni et al., 2017). In this regard, Fe-oxides may be present widely on the Moon in locations where captured oxygen or water with the presence of heating via impact or magma underplating, although this hypothesis should be further investigated.

4.3. One possible origin of nanophase metallic iron

Nanophase metallic iron (Fe^0) is a common mineral in lunar regolith, highland breccias, and meteorites (Tsay et al., 1973; Noble and Pieters, 2002; Papike et al., 1998; Wang et al., 2012; Wu et al., 2017). The metallic iron in lunar samples could be produced by magma crystallization (Hewins and Goldstein, 1974), subsolidus reduction of Fe—Ti spinel, ilmenite, and fayalite (El Goresy and Ramdohr, 1975; Noguchi et al., 2011; Ramdohr and Goresey, 1970), space weathering (Pieters et al., 2000), or impact-induced decomposition of pyroxene (Guo et al., 2020) and fayalite (Guo et al., 2022).

This study presents an additional potential mechanism for metallic iron formation. Our results show that troilite is easily oxidized when irradiated in air, reflecting the fragility of its crystal structure. A 1.50 mW laser power is enough for the distortion of the troilite structure in both air and vacuum. With increasing laser energy, the typical Raman peaks of the S—S vibrations (148 cm^{-1} and 196 cm^{-1}) in troilite disappear (Fig. 10), directly pointing to the loss of S. The metastable intermediate phase occurring at stage I in Fig. 10 would further decompose with increasing laser energy, as the Raman peaks in the Fe—S region gradually become weak and simple. As sulfur is one of the

volatile elements being more mobile than iron (Tachibana and Huss, 2005; Matsumoto et al., 2021), it would most likely have steamed away during laser irradiation. High-temperature conditions induced by laser irradiation would put the Fe—S bond in an excited state. Without oxygen, Fe^{2+} in troilite can only tend to be reduced to Fe^0 after the volatilization of sulfur. Therefore, we propose that the following reaction series (Harries and Langenhorst, 2013) may occur in vacuum environment:

$$FeS = xFe^0 + 1 - x\ (FeS) + xS\uparrow \quad (5)$$

However, no nanophase metallic Fe^0 was detected around the laser spot (Fig. 3–b), probably due to the small amount or small particle size of the newly formed Fe^0. The formed nano Fe^0 may be packaged by the S steam and deposit in different places of sample surface, or extracted in vacuum. This mechanism can interpret that metallic Fe^0 (or Fe—Ni alloy) is always associated with troilite (Fig. 1) (Berger et al., 2011; Buz et al., 2015). Furthermore, troilite had been found in some shock-melt veins (Bennett III and McSween, 1996; Chen et al., 2002), with partial migration of S (Tomkins, 2009), also implying that impact thermal desulphurization of troilite indeed occurred.

In the most recent study of the Chang'E-5 lunar samples, elongated nanophase metallic Fe^0 particles were observed for the first time throughout the interior of the troilite grain (Gu et al., 2022). Since solar wind irradiation and UV radiation usually damage the top surface of the grain, the temperature may alter the whole grain at a certain depth. Therefore, one possible reason for the formation of the nanophase metallic Fe^0 particles and the vesicle of the troilite can be attributed to thermal issues. In summary, our experiments indicate that troilite could be the source of metallic Fe^0 via a high temperature-induced S volatilization process, such as impact heating (Guo et al., 2020), magma underplating (Glotch et al., 2010), and ion irradiation (Laczniak et al., 2021).

4.4. Implications for evaluating a long-lived dynamo of the Moon

Whether the Moon has a long-lived magnetosphere is a highly debated issue. Many paleomagnetic measurements of Apollo samples support that the Moon once had a core dynamo generating surface field intensities comparable to that of Earth today (Cournède et al., 2012; Garrick-Bethell et al., 2009; Garrick-Bethell et al., 2017; Maurice et al., 2020; Rochette et al., 2010; Weiss and Tikoo, 2014). The lifetime of the dynamo was proposed to be lasting from at least 4.2 to <2.0 Ga ago (Mighani et al., 2020). However, a recent measurement shows that magnetic signals of lunar samples may come from the transient field generated by impacts and thus argues against the presence of a long-lived core dynamo (Tarduno et al., 2021). Recovering reliable paleointensities from primary magnetic records of lunar samples is thus critical to evaluating the presence or absence of long-lived dynamo of the Moon.

One of the most broadly accepted paleointensity techniques is comparing the thermal remanent magnetization acquired in the laboratory to the original natural remanent magnetization of the sample, which needs to heat the sample to high temperatures, e.g., magnetic measurements using thermal paleointensity techniques commonly heated lunar samples up to 700 °C (Tarduno et al., 2021; Tikoo et al., 2017). Thermal alteration during heating may change the sample's magnetic carrying capacity, thus hindering the acquirement of reliable paleointensity results (Fau et al., 2019). Troilite is an antiferromagnetic mineral at room temperature and thus cannot record the remanence of magnetic field. However, our study shows that it can either reduce to iron or oxidize to magnetite and/or hematite, which are ferro/ferrimagnetic minerals with strong magnetic carrying capacity, thus modifying the sample's magnetic properties. Therefore, the thermally induced phase transition of troilite observed in this study provides intuitive evidence for potential magnetic alteration during heating, reminding us that proper control of the oxidation-reduction environment during thermal paleointensity measurements is essential for achieving reliable paleointensity of samples recovered from the Moon and other planetary bodies. In addition, impact, magma underplating, and alteration during analysis would also have the potential to change lunar samples' magnetic properties. Any model for the presence or absence of long-lived dynamo of the Moon needs to consider the thermal effects on the phase transition of troilite.

5. Conclusions

High laser power has slightly decreased the frequencies of the Raman peaks of pyrite and magnetite but not for hematite. Also, pyrite and magnetite may be oxidized to hematite under laser irradiation, resulting in erroneous interpretations of the minerals phase.

Raman spectra with high quality of the troilite obtained from the one heated in air and the one heated in vacuum exhibited peaks at 148 cm^{-1}, 196– 197 cm^{-1}, 226– 228 cm^{-1}, 255 cm^{-1}, and broad peaks at 300– 335 cm^{-1}. Special attention should be paid to the Raman measurement and the preservation of Fe-bearing minerals, especially troilite. Appropriate laser energy and atmospheric environment should be provided. For 532 nm laser, irradiation on the sample of 8 mW/μm^2 is the appropriate laser power value for Raman spectroscopy of troilite. It can be transformed into magnetite and hematite if the laser power is beyond 12 mW/μm^2.

All these observations suggest that troilite may serve as the precursor for the nanophase metallic Fe^0 and magnetite of the Moon. Heating generated by impact or magma underplating would change lunar troilite to magnetic minerals (Fe^0 or magnetite) and thus potentially record core dynamo-like fields. Therefore, evaluating a long-lived lunar paleomagnetosphere should preclude the influence of thermally induced phase transition of troilite.

Declaration of Competing Interest

The authors declare no competing financial interest.

Data availability

Data will be made available on request.

Acknowledgments

This work was funded by the Key Research Program of the Chinese Academy of Sciences (ZDBS-SSW-JSC007-15), the pre-research project on Civil Aerospace Technologies of China National Space Administration (D020203), the Key Research Program (IGGCAS-202101), and the Experimental Technology Innovation Fund of the Institute of Geology and Geophysics, Chinese Academy of Sciences, Grant NO.E0518504.

References

Avril, C., Malavergne, V., Caracas, R., Zanda, B., Reynard, B., Charon, E., Bobocioiu, E., Brunet, F., Borensztajn, S., Pont, S., Tarrida, M., Guyot, F., 2013. Raman spectroscopic properties and Raman identification of CaS-MgS-MnS-FeS-Cr2FeS4 sulfides in meteorites and reduced sulfur-rich systems. Meteorit. Planet. Sci. 48 (8), 1415–1426.

Barboni, M., Boehnke, P., Keller, B., Kohl, I.E., Schoene, B., Young, E.D., McKeegan, K.D., 2017. Early formation of the moon 4.51 billion years ago. Sci. Adv. 3 (1), 1–8 e1602365.

Begemann, F., Wlotzka, F., 1969. Shock induced thermal metamorphism and mechanical deformations in the Ramsdorf chondrite. Geochim. Cosmochim. Acta 33 (11), 1351–1370.

Bell, P., El Goresy, A., Mao, H., 1974. A study of iron-rich particles on the surfaces of orange glass spheres from 74220. In: Proc. Lunar Sci. Conf. 5th, pp. 187–191.

Bennett III, M.E., McSween, H.Y., 1996. Shock features in iron-nickel metal and troilite of L-group ordinary chondrites. Meteorit. Planet. Sci. 31 (2), 255–264.

Berger, E.L., Zega, T.J., Keller, L.P., Lauretta, D.S., 2011. Evidence for aqueous activity on comet 81P/wild 2 from sulfide mineral assemblages in stardust samples and CI chondrites. Geochim. Cosmochim. Acta 75 (12), 3501–3513.

Boctor, N.Z., Bell, P.M., Mao, H.K., Kullerud, G., 1982. Petrology and shock metamorphism of Pampa del Infierno chondrite. Geochim. Cosmochim. Acta 46 (10), 1903–1911.
Brounce, M., Boyce, J., McCubbin, F.M., Humphreys, J., Reppart, J., Stolper, E., Eiler, J., 2019. The oxidation state of sulfur in lunar apatite. Am. Mineral. 104 (2), 307–312.
Bryant, R.N., Pasteris, J.D., Fike, D.A., 2018. Variability in the Raman Spectrum of unpolished growth and fracture surfaces of pyrite due to laser heating and crystal orientation. Appl. Spectrosc. 72 (1), 37–47.
Buz, J., Weiss, B.P., Tikoo, S.M., Shuster, D.L., Gattacceca, J., Grove, T.L., 2015. Magnetism of a very young lunar glass. J. Geophys. Res.: Planets 120 (10), 1720–1735.
Cameron, E.N., 1970. Opaque minerals in lunar samples. Science 167 (3918), 623–625.
Carpenter, R.H., Desborough, G.A., 1964. Range in solid solution and structure of naturally occurring troilite and pyrrhotite. Am. Mineral. 49 (9–10), 1350–1365.
Chen, M., Xie, X., Wang, D., Wang, S., 2002. Metal-troilite-magnetite assemblage in shock veins of Sixiangkou meteorite. Geochim. Cosmochim. Acta 66 (17), 3143–3149.
Cournède, C., Gattacceca, J., Rochette, P., 2012. Magnetic study of large Apollo samples: possible evidence for an ancient centered dipolar field on the moon. Earth Planet. Sci. Lett. 331-332, 31–42.
Dąbrowski, A., Mendyk, E., Robens, E., Skrzypiec, K., Goworek, J., Iwan, M., Rzączyńska, Z., 2008. Investigation of surface properties of lunar regolith part III. J. Therm. Anal. Calorim. 94 (3), 633–639.
de Faria, D.L.A., Lopes, F.N., 2007. (Heated goethite and natural hematite): can Raman spectroscopy be used to differentiate them? Vib. Spectrosc. 45 (2), 117–121.
de Faria, D.L.A., Venâncio, Silva S., de Oliveira, M.T., 1997. Raman microspectroscopy of some iron oxides and oxyhydroxides. J. Raman Spectrosc. 28 (11), 873–878.
El Goresy, A., 2018. In: Douglas, R. (Ed.), Oxide Minerals. In Chapter 5. Oxide Minerals in Lunar Rocks. De Gruyter, pp. 213–258.
El Goresy, A., Ramdohr, P., 1975. Subsolidus reduction of lunar opaque oxides-textures, assemblages, geochemistry, and evidence for a late-stage endogenic gaseous mixture. In: Proc. Lunar Sci. Conf. 6th, pp. 729–745.
Evans, H.T., 1970. Lunar troilite: crystallography. Science 167 (3918), 621–623.
Fagents, S.A., Elise, Rumpf M., Crawford, I.A., Joy, K.H., 2010. Preservation potential of implanted solar wind volatiles in lunar paleoregolith deposits buried by lava flows. Icarus 207 (2), 595–604.
Fau, A., Beyssac, O., Gauthier, M., Meslin, P.Y., Cousin, A., Benzerara, K., Bernard, S., Boulliard, J.C., Gasnault, O., Forni, O., Wiens, R.C., Morand, M., Rosier, P., Garino, Y., Pont, S., Maurice, S., 2019. Pulsed laser-induced heating of mineral phases: implications for laser-induced breakdown spectroscopy combined with Raman spectroscopy. Spectrochim. Acta B At. Spectrosc. 160 (105687.1-14).
Fei, Y., Bertka, C.M., Finger, L.W., 1997. High-pressure Iron-sulfur compound, Fe3S2, and melting relations in the Fe-FeS system. Science 275 (5306), 1621–1623.
Fleet, M., 1970. Structural aspects of the marcasite-pyrite transformation. Can. Mineral. 10 (2), 225–231.
Forester, D., 1973. Mössbauer search for ferric oxide phases in lunar materials and simulated lunar materials. In: Proc. Lunar Sci. Conf. 4th, pp. 2697–2707.
Foucher, F., 2022. Influence of laser shape on thermal increase during micro-Raman spectroscopy analyses. J. Raman Spectrosc. 53 (3), 664–676.
Garrick-Bethell, I., Weiss, B.P., Shuster, D.L., Buz, J., 2009. Early lunar magnetism. Science 323 (5912), 356–359.
Garrick-Bethell, I., Weiss, B.P., Shuster, D.L., Tikoo, S.M., Tremblay, M.M., 2017. Further evidence for early lunar magnetism from troctolite 76535. J. Geophys. Res.: Planets 122 (1), 76–93.
Genchev, G., Erbe, A., 2016. Raman spectroscopy of Mackinawite FeS in anodic Iron sulfide corrosion products. J. Electrochem. Soc. 163 (6), C333–C338.
Glotch, T.D., Lucey, P.G., Bandfield, J.L., Greenhagen, B.T., Thomas, I.R., Elphic, R.C., Bowles, N., Wyatt, M.B., Allen, C.C., Hanna, K.D., 2010. Highly silicic compositions on the moon. science 329 (5998), 1510–1513.
Griscom, D., Marquardt, C., 1972. Evidence of lunar surface oxidation processes: Electron spin resonance spectra of lunar materials and simulated lunar materials. In: Proc. Lunar Sci. Conf. 3rd, pp. 2397–2415.
Gu, L., Chen, Y., Xu, Y., Tang, X., Lin, Y., Noguchi, T., Li, J., 2022. Space weathering of the Chang'e-5 lunar sample from a mid-high latitude region on the moon. Geophys. Res. Lett. 49 (7) (e2022GL097875).
Guo, Z., Li, Y., Liu, S., Xu, H., Xie, Z., Li, S., Li, X., Lin, Y., Coulson, I.M., Zhang, M., 2020. Discovery of nanophase iron particles and high pressure clinoenstatite in a heavily shocked ordinary chondrite: implications for the decomposition of pyroxene. Geochim. Cosmochim. Acta 272, 276–286.
Guo, Z., Li, C., Li, Y., Wen, Y., Tai, K., Li, X., Liu, J., Ouyang, Z., 2022. Nanophase Iron particles derived from Fayalitic olivine decomposition in Chang'E-5 lunar soil: implications for thermal effects during impacts. Geophys. Res. Lett. 49 (5) (e2021GL097323).
Hanesch, M., 2009. Raman spectroscopy of iron oxides and (oxy. hydroxides at low laser power and possible applications in environmental magnetic studies). Geophys. J. Int. 177 (3), 941–948.
Harries, D., Langenhorst, F., 2013. The nanoscale mineralogy of Fe,Ni sulfides in pristine and metamorphosed CM and CM/CI-like chondrites: Tapping a petrogenetic record. Meteorit. Planet. Sci. 48 (5), 879–903.
Hewins, R.H., Goldstein, J.I., 1974. Metal-olivine associations and NiCo contents in two Apollo 12 mare basalts. Earth Planet. Sci. Lett. 24 (1), 59–70.
Jacob, D.E., Kronz, A., Viljoen, K.S., 2004. Cohenite, native iron and troilite inclusions in garnets from polycrystalline diamond aggregates. Contrib. Mineral. Petrol. 146 (5), 566–576.
Joy, K.H., Visscher, C., Zolensky, M.E., Mikouchi, T., Hagiya, K., Ohsumi, K., Kring, D.A., 2015. Identification of magnetite in lunar regolith breccia 60016: evidence for oxidized conditions at the lunar surface. Meteorit. Planet. Sci. 50 (7), 1157–1172.
Kolopus, J., Kline, D., Chatelain, A., Weeks, R., 1971. Magnetic resonance properties of lunar samples: mostly Apollo 12. In: Proc. Lunar Sci. Conf. 2nd, pp. 2501–2514.
Laczniak, D.L., Thompson, M.S., Christoffersen, R., Dukes, C.A., Clemett, S.J., Morris, R. V., Keller, L.P., 2021. Characterizing the spectral, microstructural, and chemical effects of solar wind irradiation on the Murchison carbonaceous chondrite through coordinated analyses. Icarus 364, 114479.
Ling, Z.C., Wang, A., Jolliff, B.L., 2011. Mineralogy and geochemistry of four lunar soils by laser-Raman study. Icarus 211 (1), 101–113.
Liu, J., Xu, A., Meng, Y., He, Y., Ren, P., Guo, W.-P., Peng, Q., Yang, Y., Jiao, H., Li, Y., Wen, X.-D., 2019. From predicting to correlating the bonding properties of iron sulfide phases. Comput. Mater. Sci. 164, 99–107.
Marshall, C.P., Marshall, A.O., 2011. Hematite and carbonaceous materials in geological samples: a cautionary tale. Spectrochim. Acta A Mol. Biomol. Spectrosc. 80 (1), 133–137.
Matamoros-Veloza, A., Cespedes, O., Johnson, B.R.G., Stawski, T.M., Terranova, U., de Leeuw, N.H., Benning, L.G., 2018. A highly reactive precursor in the iron sulfide system. Nat. Commun. 9 (1), 3125.
Matsumoto, T., Noguchi, T., Tobimatsu, Y., Harries, D., Langenhorst, F., Miyake, A., Hidaka, H., 2021. Space weathering of iron sulfides in the lunar surface environment. Geochim. Cosmochim. Acta 299, 69–84.
Maurice, M., Tosi, N., Schwinger, S., Breuer, D., Kleine, T., 2020. A long-lived magma ocean on a young moon. Sci. Adv. 6 (28), eaba8949.
Mernagh, T.P., Trudu, A.G., 1993. A laser Raman microprobe study of some geologically important sulphide minerals. Chem. Geol. 103 (1), 113–127.
Mighani, S., Wang, H., Shuster, D.L., Borlina, C.S., Nichols, C.I.O., Weiss, B.P., 2020. The end of the lunar dynamo. Sci. Adv. 6 (1), eaax0883.
Minitti, M.E., Lane, M.D., Bishop, J.L., 2005. A new hematite formation mechanism for Mars. Meteorit. Planet. Sci. 40 (1), 55–69.
Mitchell, R.E., 2002. Mechanisms of Pyrite Oxidation to Non-slagging Species. Stanford University (US).
Miyahara, M., Yamaguchi, A., Saitoh, M., Fukimoto, K., Sakai, T., Ohfuji, H., Tomioka, N., Kodama, Y., Ohtani, E., 2020. Systematic investigations of high-pressure polymorphs in shocked ordinary chondrites. Meteorit. Planet. Sci. 55 (12), 2619–2651.
Moldenhauer, H., Bayer, M., Debus, J., Nikolov, A., Brümmer, A., 2018. Raman scattering study of micrometer-sized spots of magnetite and hematite formed at 18CrNiMo7-6 screw rotor surfaces due to liquid-free, unsynchronized operation. IOP Conf. Ser.: Mater. Sci. Eng. 425, 012016.
Moreau, J.-G., Jõeleht, A., Aruväli, J., Heikkilä, M.J., Stojic, A.N., Thomberg, T., Plado, J., Hietala, S., 2022. Bulk synthesis of stoichiometric/meteoritic troilite (FeS) by high-temperature pyrite decomposition and pyrrhotite melting. Meteorit. Planet. Sci. 57 (3), 588–602.
Münker, C., Fonseca, R.O.C., Schulz, T., 2017. Silicate Earth's missing niobium may have been sequestered into asteroidal cores. Nat. Geosci. 10 (11), 822–826.
Neuville, D.R., de Ligny, D., Henderson, G.S., 2014. Advances in Raman spectroscopy applied to earth and material sciences. Rev. Mineral. Geochem. 78 (1), 509–541.
Nickel, E.H., 1968. Structural stability of minerals with the pyrite, marcasite, arsenopyrite and lollingite structures. Can. Mineral. 9 (3), 311–321.
Noble, S.K., Pieters, C.M., 2002. The Optical Effects of Space Weathering Products on Silicate Surfaces, P61A. Am. Geophys. Union, 0339-0339.
Noguchi, T., Nakamura, T., Kimura, M., Zolensky, M., Tanaka, M., Hashimoto, T., Konno, M., Nakato, A., Ogami, T., Fujimura, A., 2011. Incipient space weathering observed on the surface of Itokawa dust particles. Science 333 (6046), 1121–1125.
Onufrienok, V.V., Chzhan, A.V., Bondarenko, G.V., Yurkin, G.Y., 2020. Transition of metastable Pyrrhotites to a stable phase state. Inorg. Mater. 56 (9), 898–902.
Owens, F.J., Orosz, J., 2006. Effect of nanosizing on lattice and magnon modes of hematite. Solid State Commun. 138 (2), 95–98.
Papike, J.J., Ryder, G., Shearer, C.K., 1998. Lunar samples. Rev. Mineral. Geochem. 36 (1), 189.
Pasieczna-Patkowska, S., Dąbrowski, A., Robens, E., Ryczkowski, J., 2008. FT-IR/PAS studies of lunar regolith samples. Acta Phys. Pol., A. Opt. and Acoust. Methods Sci. Technol. 114, A163–A168.
Pieters, C.M., Taylor, L.A., Noble, S.K., Keller, L.P., Hapke, B., Morris, R.V., Allen, C.C., Mckayd, S., Wentworth, S., 2000. Space weathering on airless bodies: resolving a mystery with lunar samples. Meteorit. Planet. Sci. 35 (5), 1101–1107.
Prieto-delaVega, I., García-Florentino, C., Torre-Fdez, I., Huidobro, J., Aramendia, J., Arana, G., Castro, K., Madariaga, J.M., 2022. Original and alteration mineral phases in the NWA 10628 Martian shergottite determined by micro-Raman spectroscopy assisted with micro-energy dispersive X-ray fluorescence imaging. J. Raman Spectrosc. 53 (3), 435–449.
Prince, B.S., Magnuson, M.P., Chaves, L.C., Thompson, M.S., Loeffler, M.J., 2020. Space weathering of FeS induced via pulsed laser irradiation. J. Geophys. Res.: Planets 125 (5), 1–14.
Qian, G., Brugger, J., Skinner, W.M., Chen, G., Pring, A., 2010. An experimental study of the mechanism of the replacement of magnetite by pyrite up to 300°C. Geochim. Cosmochim. Acta 74 (19), 5610–5630.
Ramdohr, P., Goresey, A.E., 1970. Opaque minerals of the lunar rocks and dust from Mare Tranquillitatis. Science 167 (3918), 615–618.
Rochette, P., Gattacceca, J., Ivanov, A.V., Nazarov, M.A., Bezaeva, N.S., 2010. Magnetic properties of lunar materials: meteorites, Luna and Apollo returned samples. Earth Planet. Sci. Lett. 292 (3), 383–391.

Runcorn, S.K., Collinson, D., O'Reilly, W., Stephenson, A., Battey, M., Manson, A., Readman, P., 1971. Magnetic properties of Apollo 12 lunar samples. Proc. R. Soc. Lond. A. Math. Phys. Sci. 325 (1561), 157–174.
Sahoo, S., Gaur, A.P.S., Ahmadi, M., Guinel, M.J.F., Katiyar, R.S., 2013. Temperature-dependent Raman studies and thermal conductivity of few-layer MoS2. J. Phys. Chem. C 117 (17), 9042–9047.
Schaible, M.J., Pinto, H.P., McKee, A.D., Leszczynski, J., Orlando, T.M., 2019. Characterization and simulation of natural pyrite surfaces: a combined experimental and theoretical study. J. Phys. Chem. C 123 (43), 26397–26405.
Scott, E.R.D., 1982. Origin of rapidly solidified metal-troilite grains in chondrites and iron meteorites. Geochim. Cosmochim. Acta 46 (5), 813–823.
Sharma, S.K., Misra, A.K., Lucey, P.G., Lentz, R.C.F., 2009. A combined remote Raman and LIBS instrument for characterizing minerals with 532nm laser excitation. Spectrochim. Acta A Mol. Biomol. Spectrosc. 73 (3), 468–476.
Shearer, C.K., Sharp, Z.D., Burger, P.V., McCubbin, F.M., Provencio, P.P., Brearley, A.J., Steele, A., 2014. Chlorine distribution and its isotopic composition in "rusty rock" 66095. Implications for volatile element enrichments of "rusty rock" and lunar soils, origin of "rusty" alteration, and volatile element behavior on the moon. Geochim. Cosmochim. Acta 139, 411–433.
Shebanova, O.N., Lazor, P., 2003. Raman spectroscopic study of magnetite (FeFe2O4): a new assignment for the vibrational spectrum. J. Solid State Chem. 174 (2), 424–430.
Skinner, B.J., Luce, F.D., 1971. Solid solutions of the type (Ca,Mg,Mn,Fe) S and their use as geothermometers for the enstatite chondrites. Am. Mineral. 56 (7–8), 1269–1296.
Skinner, W.M., Nesbitt, H.W., Pratt, A.R., 2004. XPS identification of bulk hole defects and itinerant Fe 3d electrons in natural troilite (FeS). Geochim. Cosmochim. Acta 68 (10), 2259–2263.
Stöffler, D., Keil, K., Edward, S., 1991. Shock metamorphism of ordinary chondrites. Geochim. Cosmochim. Acta 55 (12), 3845–3867.
Tachibana, S., Huss, G.R., 2003. The initial abundance of 60 Fe in the solar system. Astrophys. J. 588 (1), L41–L44.
Tachibana, S., Huss, G.R., 2005. Sulfur isotope composition of putative primary troilite in chondrules from Bishunpur and Semarkona. Geochim. Cosmochim. Acta 69 (12), 3075–3097.
Tarduno, J.A., Cottrell, R.D., Lawrence, K., Bono, R.K., Huang, W., Johnson, C.L., Blackman, E.G., Smirnov, A.V., Nakajima, M., Neal, C.R., Zhou, T., Ibanez-Mejia, M., Oda, H., Crummins, B., 2021. Absence of a long-lived lunar paleomagnetosphere. Sci. Adv. 7 (32), eabi7647.
Taylor, L.A., Burton, J.C., 1976. Experiments on the stability of FeOOH on the surface of the moon. Meteoritics 11 (3), 225–230.
Taylor, L.A., Mao, H.K., Bell, P.M., 1974. Identification of the hydrated Iron oxide mineral Akaganéite in Apollo 16 lunar rocks. Geology 2 (9), 429–432.
Terada, K., Yokota, S., Saito, Y., Kitamura, N., Asamura, K., Nishino, M.N., 2017. Biogenic oxygen from earth transported to the moon by a wind of magnetospheric ions. Nature Astronomy 1 (2), 0026.
Terranova, U., Mitchell, C., Sankar, M., Morgan, D., de Leeuw, N.H., 2018. Initial oxygen incorporation in the prismatic surfaces of Troilite FeS. J. Phys. Chem. C 122 (24), 12810–12818.
Thomas, J.E., Skinner, W.M., R. S. t. C. Smart., 2003. A comparison of the dissolution behavior of troilite with other iron(II) sulfides; implications of structure. Geochim. Cosmochim. Acta 67 (5), 831–843.
Tikoo, S.M., Weiss, B.P., Shuster, D.L., Suavet, C., Wang, H., Grove, T.L., 2017. A two-billion-year history for the lunar dynamo. Sci. Adv. 3 (8), e1700207.
Tomkins, A.G., 2009. What metal-troilite textures can tell us about post-impact metamorphism in chondrite meteorites. Meteorit. Planet. Sci. 44 (8), 1133–1149.
Tsay, Fun-Dow, Manatt, S.L., Chan, S.I., 1973. (Magnetic phases in lunar fines): metallic Fe or ferric oxides? Geochim. Cosmochim. Acta 37 (5), 1201–1211.
Udayabhaskar, Reddy G., Seshamaheswaramma, K., Nakamura, Y., Lakshmi, Reddy S., Frost, R.L., Endo, T., 2012. Electron paramagnetic resonance, optical absorption and Raman spectral studies on a pyrite/chalcopyrite mineral. Spectrochim. Acta A Mol. Biomol. Spectrosc. 96, 310–315.
von Steiger, R., Zurbuchen, T.H., McComas, D.J., 2010. Oxygen flux in the solar wind: Ulysses observations. Geophys. Res. Lett. 37 (22).
Wadhwa, M., 2008. Redox conditions on small bodies, the moon and Mars. Rev. Mineral. Geochem. 68 (1), 493–510.
Wang, A., Jolliff, B.L., Haskin, L.A., 1999. Raman spectroscopic characterization of a Martian SNC meteorite: Zagami. J. Geophys. Res.: Planets 104 (E4), 8509–8519.
Wang, A., Kuebler, K.E., Jolliff, B.L., Haskin, L.A., 2004. Raman spectroscopy of Fe-Ti-Cr-oxides, case study: Martian meteorite EETA79001. Am. Mineral. 89 (5–6), 665–680.
Wang, K., Moynier, F., Podosek, F.A., Foriel, J., 2012. An iron isotope perspective on the origin of the nanophase metallic iron in lunar regolith. Earth Planet. Sci. Lett. 337-338, 17–24.
Wang, A., Korotev, R.L., Jolliff, B.L., Ling, Z., 2015. Raman imaging of extraterrestrial materials. Planet. Space Sci. 112, 23–34.
Weber, I., Böttger, U., Pavlov, S.G., Hübers, H.-W., Hiesinger, H., Jessberger, E.K., 2017. Laser alteration on iron sulfides under various environmental conditions. J. Raman Spectrosc. 48 (11), 1509–1517.
Weeks, R., 1972. Magnetic phases in lunar material and their electron magnetic resonance spectra: Apollo 14. In: Proc. Lunar Sci. Conf. 3rd, pp. 2503–2517.
Weeks, R., Kolopus, J., Kline, D., Chatelain, A., 1970. Apollo 11 lunar material: Nuclear magnetic resonance of 27Al and electron resonance of Fe and Mn. Geochim. Cosmochim. Acta Suppl. 1, 2467–2490.
Weeks, R., Kolopus, J., Kline, D., 1972. Magnetic phases in lunar material and their Electron magnetic resonance spectra: Apollo 14. In Lunar and Planetary Science Conference 791–793.
Weiss, B.P., Tikoo, S.M., 2014. The lunar dynamo. Science 346 (6214), 1246753.
Wesełucha-Birczyńska, A., Żmudzka, M., 2008. Micro-Raman spectroscopy characterization of selected meteorites. J. Mol. Struct. 887 (1), 253–261.
White, S.N., 2009. Laser Raman spectroscopy as a technique for identification of seafloor hydrothermal and cold seep minerals. Chem. Geol. 259 (3), 240–252.
Wopenka, B., 2012. (Raman spectroscopic investigation of two grains from comet 81P/Wild 2): information that can be obtained beyond the presence of sp2-bonded carbon. Meteorit. Planet. Sci. 47 (4), 565–584.
Wu, Y., Li, X., Yao, W., Wang, S., 2017. Impact characteristics of different rocks in a pulsed laser irradiation experiment: simulation of micrometeorite bombardment on the moon. J. Geophys. Res.: Planets 122 (10), 1956–1967.
Zhou, G., Shan, Y., Wang, L., Hu, Y., Guo, J., Hu, F., Shen, J., Gu, Y., Cui, J., Liu, L., Wu, X., 2019. Photoinduced semiconductor-metal transition in ultrathin troilite FeS nanosheets to trigger efficient hydrogen evolution. Nat. Commun. 10 (1), 399.